Astron. Astrophys. 342, 395–407 (1999)

ASTRONOMY AND ASTROPHYSICS

A complex Lyman limit system at $z = 1.9$ towards HS 1103+6416⋆

S. Köhler[1], **D. Reimers**[1], **D. Tytler**[2], **H.-J. Hagen**[1], **T. Barlow**[3], **and S. Burles**[4]

[1] Hamburger Sternwarte, Universität Hamburg, Gojenbergsweg 112, D-21029 Hamburg, Germany
[2] Center for Astrophysics and Space Sciences, University of California, San Diego, C-0424, La Jolla, CA 92093, USA
[3] IPAC/Caltech, M/S 100-22, 770 South Wilson Ave., Pasadena, CA 91125, USA
[4] Department of Astronomy and Astrophysics, University of Chicago, 5640 S. Ellis Ave, Chicago, IL 60637, USA

Received 17 March 1998 / Accepted 28 October 1998

Abstract. We analyse absorption lines in optical and ultraviolet spectra of the bright ($V = 15.8$, $z = 2.19$) QSO HS 1103+6416. High-resolution (FWHM $= 8$ km s^{-1}) optical spectra have been obtained with the Keck 10 m telescope in the range from 3180 to 5780 Å. Ultraviolet observations in the range from 1150 to 3280 Å were performed with the FOS and the GHRS onboard the Hubble Space Telescope (HST). In this paper we concentrate our discussion on a complex Lyman limit system (LLS) at $z = 1.89$. Absorption lines by carbon, silicon and aluminum in the optical spectra reveal a complex velocity structure with at least 11 components spanning a velocity range of 200 km s^{-1}. From the Lyman limit in the ultraviolet spectra we derive a total neutral hydrogen column density of $\log N(\mathrm{H\,I}) = 17.46$ cm^{-2}.

Column densities of heavy elements in the individual components were derived by Voigt profile fitting. The eleven components can be subdivided roughly into three groups: Components 2, 3 and 6 with radial velocities v = -129... -95 km s^{-1} with low ionization (L), components 4, 5, 7, 8 (v = -75... $+2$) with intermediate ionization (I), and components 1, 9, 10, 11 (v = -129, $+34$... $+57$) with high ionization (H). In order to study the ionization and abundances in these systems we compare the observed column densities with photoionization models. The observed absorption in the optical data can be explained by individual clouds with slightly varying metal abundances photoionized by slightly different radiation fields. Highly ionized components favour the extragalactic radiation field as calculated by Haardt & Madau (1996) while the components of low and intermediate ionization are better reproduced with a harder ionizing radiation field. Obviously local sources like stars can therefore be excluded as the main ionizing sources.

Abundances in components L and I appear to be slightly different from those in the high ionization component H.

In L and I we find roughly [C/H] = -0.9 while H has [C/H] = -1.2, consistent with the expectation that in a galaxy or groups of galaxies the abundances in the higher ionized 'Halo' component are lower. The relative element abundances are also different. While in components L and I [Si/C] ≈ 0.2, barely significant, and [S/C] and [O/C] ≈ 0 within the uncertainties, component H shows [Si/C] = 0.5 and in addition [O/C] and [S/C] = 0.4 (both from HST spectra). [Al/C] measurable only in L and I is always ≈ 0.

The tendency of enhanced α element (O, Si, S) abundances at low C abundance is consistent with what is known from nucleosynthesis theory (SNII dominant at the beginning of galactic evolution), from metal deficient stars in our galaxy and from QSO absorption line systems. If all components were ionized by the same radiation field the relative overabundances of O and S in the highly ionized components would be even larger.

We show that HS 1103+6416 will offer in the future for the first time the possibility to measure the cosmic He abundance at high redshift. Detailed calculations of He I absorption using the multicomponent model which explains the metal lines shows consistency with the observed first seven series members of the He I 584, 537, 522 Å ... series for a helium abundance $Y = 0.24$, the expected cosmic He abundance from Big Bang nucleosynthesis modified by stellar nucleosynthesis at $\sim 1/10$ solar metallicity.

The presence of O I and possibly O VI absorption cannot be explained by our photoionization models and might hint at the existence of additional mainly neutral components with relatively low H I column density and further ionization mechanisms like, e.g., collisional ionization.

Key words: cosmology: observations – galaxies: quasars: individual: HS 1103+6416 – galaxies: quasars: general – galaxies: quasars: absorption lines

1. Introduction

Quasar absorption lines offer a unique possibility to study the physical properties of intervening gas clouds as well as the metagalactic UV radiation field at higher redshifts. The highly ionized absorber systems have only few resonance absorption lines like C IV 1550, Si IV 1400, N V 1240, O VI 1334 accessible

Send offprint requests to: D. Reimers

⋆ Based on observations with the NASA/ESA Hubble Space Telescope, obtained at the Space Telescope Science Institute, which is operated by Aura, Inc., under NASA contract NAS 5–26 555. Optical data presented herein were obtained at the W.M. Keck Observatory, which is operated as a scientific partnership among the California Institute of Technology, the University of California and the National Aeronautics and Space Administration. The Observatory was made possible by the generous financial support of the W.M. Keck Foundation.

Correspondence to: dreimers@hs.uni-hamburg.de

Table 1. Observational parameters for HST spectra of HS 1103+6416.

Detector/Grating	Exposure time [s]	Resolution FWHM [Å]	Observed range [Å]	Date	Offset [Å]	S/N_{max}
AMBER/G270H	5336	2	2223–3277	Oct 31 1995	0.5	46
AMBER/G190H	8628	1.44	1572–2311	Oct 31 1995	1.24	21
DET1/G140L	17408	0.77	1415–1700	Jul 9 1996	0.66	8
DET1/G140L	22739	0.77	1150–1436	Jul 9 1996	0.66	12

from the ground in high redshift QSOs. Nearly all strong resonance lines of abundant ions (O III–O V, Ne III–Ne VIII, S III–S V, N III–N IV etc.) are in the intrinsic EUV part of the spectrum. This means, that abundance studies in the highly ionized component of the IGM of elements like O, Ne, S or N require the observation of the intrinsic EUV spectra of high-redshift QSOs.

In ultraviolet spectra obtained with the Hubble Space Telescope (HST) of the UV-bright, high-redshift ($z = 2.72$) QSO HS 1700+6416 we detected at least 16 heavy-element absorption systems thereby 7 Lyman limit systems (LLS). Prominent absorption lines which have been seen for the first time in a cosmic object except the Sun are: O V 629, O IV 554, 553, 608, 787, O III 702, 833, Ne IV 543, Ne V 480, 568, Ne VI 401, Ne VII 465, S III 677, 698, S IV 657, S V 786, N III 374, 685, 989 and many others (Reimers et al. 1992, Vogel & Reimers 1995, Köhler et al. 1996).

The rich absorption line spectra consisting mainly of high-ionization lines of abundant elements are in agreement with what we expected on the basis of photoionization calculations. It appears from our analysis that typically at high redshift the metallicity is low ([C/H] $\simeq -2$) with a clear tendency of increasing abundances with lower redshifts and that the abundances of O, Ne, Si, and S relative to C seem to behave as expected from nucleosynthesis in SN II explosions (Vogel & Reimers 1995; Köhler et al. 1996; Sperhake & Reimers 1997). The analysis of HS 1700+6416 data suffered from the extremely high line density in this high-redshift QSO and the lack of high-resolution optical data.

In the course of the Hamburg Quasar Survey (Hagen et al. 1995) we discovered HS 1103+6416, a quasar brighter than HS 1700+6416 and at a lower redshift of $z = 2.19$. Ultraviolet observations of HS 1103+6416 with IUE revealed flux down to 1250 Å and a strong LLS at $z \approx 1.9$ (Reimers et al. 1995a). Due to the lower redshift the absorption line density should be smaller and we obtained ultraviolet spectra with the HST to study the metal line systems (MLS).

With the limited spectral resolution achievable with HST in the UV even for the brightest high-redshift QSOs, the common splitting of strong MLSs into subcomponents is not resolved and hidden saturation effects can lead to false column densities. This difficulty can be overcome only with optical observations at the highest possible resolution in order to be able to synthesize the unresolved UV lines on the basis of splitting into subcomponents observed in the optical regime. For this purpose, a high-resolution spectrum has been taken with HIRES at the Keck 10 m telescope.

2. Observations

2.1. Optical observations

We present high resolution spectra of HS 1103+6416 obtained with the HIRES spectrograph (Vogt et al. 1994) on the W. M. Keck1 10 m telescope with a total of 3 hours exposure on the nights of 1996 May 20 and 1997 April 9. In both exposures, we used a $1.14'' \times 7.0''$ slit, which gave a resolution of 8 km s^{-1} and adequate sky coverage. On the night of April 9, we observed using the UV cross-disperser to increase efficiency at wavelengths below 4200 Å. The images were processed and the spectra were optimally extracted using an automated package (EE by T. Barlow) specifically designed for HIRES spectra. Thorium-Argon lamp images were obtained immediately after the observations to provide wavelength calibrations in each echelle order. The root-mean-square residuals in the wavelength calibration for each echelle order was less than 0.3 km s^{-1}. All wavelengths are vacuum values in the heliocentric frame. Each echelle order was continuum fitted with a Legendre polynomial to normalize the intrinsic QSO flux to unity.

2.2. Ultraviolet observations

Ultraviolet spectra of HS 1103+6416 have been obtained with the FOS and GHRS onboard the HST with apertures A-1 and LSA, respectively. Details of the observations are summarized in Table 1.

The STScI provided flux calibrated data together with the $1\,\sigma$ error in the flux of each pixel as a function of wavelength. The deduced signal-to-noise ratio is strongly wavelength dependent. Maximum signal-to-noise ratios for the observed wavelength ranges are given in Table 1. The wavelength zero point offset was determined by requiring that strong absorption lines by the interstellar medium are at rest. Since for some spectral regions too few ISM absorption lines are observed or some of them are obviously blended, we additionally compared a) absorption lines in overlapping regions of different observations and b) redshifts from Lyman series lines of strong LLS spanning different observations. We list in Table 1 the wavelength zeropoint offsets that were added to the reduced spectra.

3. Continuum definition and emission lines in the UV

First of all the UV data of HS 1103+6416 were corrected for interstellar reddening according to Seaton's law (1979) with $E(B-V) = 0.02$ corresponding to N(H I)=1.03 10^{20} cm^{-2} (Reimers et al. 1995b). This value is from the Stark HI survey (Stark et al. 1992)

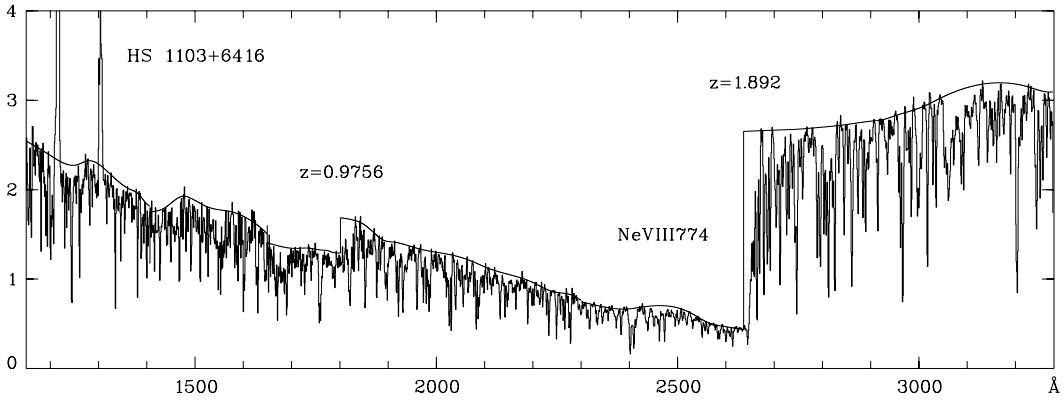

Fig. 1. Observed fluxes in 10^{-15} erg s^{-1} cm^{-2} Å^{-1} of HS1103+6416 obtained with the FOS and GHRS onboard the HST. Data have been rebinned for presentation purposes only.

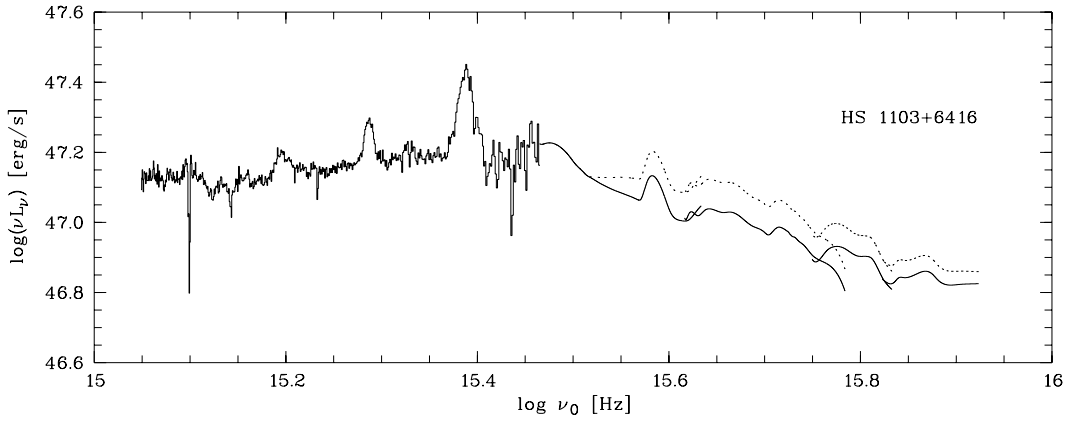

Fig. 2. Spectral energy distributions $\log(\nu\,\mathrm{L}_\nu)$ versus frequency in the rest frame of HS 1103+6416. Optical data were obtained at the Calar Alto 2.2 m telesope. In the UV the continua derived for the dereddened spectra were corrected for the neutral hydrogen continuum absorption of the LLSs and transferred to luminosities adopting $\mathrm{q}_0 = 0.5$ and $\mathrm{H}_0 = 75\,\mathrm{km\,s^{-1}\,Mpc^{-1}}$. An additional correction for the cumulative hydrogen continuum absorption of the numerous Lyα clouds with $\log N(\mathrm{H\,I}) \leq 16\,\mathrm{cm^{-2}}$ leads to higher luminosities and to changes in the continuum slopes (dotted lines).

We searched for regions in the data apparently free of absorption lines, where we calculated the mean flux and the error of the mean flux to check for consistency with the noise. The continua were then constructed by fitting cubic splines to the sample of mean flux values.

The data show one strong and one weak Lyman edge at $\lambda_{\mathrm{obs}} = 2640$ and 1800 Å, respectively (see Fig. 1). Due to blending of the highest Lyman series lines the continuum flux level is poorly defined at these edges and we manually modified the continuum in these regions. By modelling the Lyman edge and H I absorption lines calculating Voigt profiles for the first 39 Lyman series lines we find $\log N(\mathrm{H\,I})$=17.46 cm^{-2} and $b = 45\,\mathrm{km\,s^{-1}}$ for the LLS at $z = 1.892$ and $\log N(\mathrm{H\,I})$=16.6 cm^{-2} and $b = 35\,\mathrm{km\,s^{-1}}$ for the LLS at $z = 0.9756$, respectively.

The decrease in flux at $\lambda_{\mathrm{obs}} = 1450$ Å and $\lambda_{\mathrm{obs}} = 1280$ Å cannot be explained by further Lyman edges since the corresponding Lyman series lines are missing.

Since there is a large time gap between FOS and GHRS observations (8 months) we cannot decide if the observed flux increase at $\lambda_{\mathrm{obs}} = 1650$ Å is intrinsic to the QSO continuum or due to flux variations of the QSO. In the fitted continuum broad emission at $\lambda_{\mathrm{obs}} = 2490$ Å is apparent which might be due to Ne VIII 774 and/or N IV 765 and/or O IV 788.

3.1. Spectral energy distribution

Ultraviolet spectra of $z = 2$ QSOs are still strongly influenced by absorption of intervening absorbers. In order to find the intrinsic spectral energy distribution of the QSOs corrections have to be applied to the observed data. First, the dereddened spectra were corrected for continuum absorption by neutral hydrogen in the identified LLSs.

Corrected fluxes were transferred to luminosities using

$$f_{\nu 0} = 2.33\ 10^{-62}\, L_{\nu\, e}\, H_0^2 (1+z)/[(1+z)-(1+z)^{0.5}]^2$$

for $\mathrm{q}_0 = 0.5$ (Weedman 1986) and $\mathrm{H}_0 = 75\,\mathrm{km\,s^{-1}\,Mpc^{-1}}$. Fig. 2 shows the spectral energy distributions $\log(\nu\,\mathrm{L}_\nu)$ versus frequency in the rest frame of HS 1103+6416.

Monte Carlo simulations were performed in order to estimate the depression of the quasar spectrum due to the cumulative hydrogen continuum absorption by the numerous Lyα clouds.

The incidence of LLSs, i.e. absorber clouds with neutral hydrogen column densities greater than log N(H I)= $16\,\mathrm{cm}^{-2}$, is easily detected by their Lyman edges. Thus only clouds with log N(H I)$\leq 16\,\mathrm{cm}^{-2}$ are considered. The distribution in redshift and column density of Lyα clouds can be described by

$$\frac{\delta^2 N}{\delta\, N_{\mathrm{H\,I}}\, \delta\, z} = A\,(1+z)^{\gamma}\, N_{\mathrm{H\,I}}^{\beta}. \quad (1)$$

We chose A$= 2.4\,10^7$, $\gamma = 2.46$ and $\beta = -1.5$ for Lyα clouds with $2\,10^{12} \leq N(\mathrm{H\,I}) \leq 10^{16}$ (see e.g. Madau 1995 and references therein). Most absorption from Ly α lines occurs at column densities of $\sim$ log N(HI) = 14. Five thousand simulations were performed to calculate the mean transmission exp($-\tau$) at the observed wavelengths with τ given by

$$\tau(\lambda_{obs}) = \sum_{z_i \leq z_e} N(\mathrm{HI})^i \sigma(\frac{\lambda_{obs}}{1+z_i}) \quad (2)$$

and

$$\sigma(\lambda) = 6.3\;10^{-18}\,(\frac{\lambda}{\lambda_{\mathrm{LL}}})^3\,\mathrm{cm}^{-2} \quad (3)$$

for $\lambda \leq \lambda_{\mathrm{LL}} = 911.75$ Å. This additional correction leads to higher luminosities and – even more important – to changes in the continuum slope (see dotted lines in Fig. 2).

In contrast to HS 1307+4617 and HS 1700+6416 the continuum shape of HS 1103+6416 is much flatter in the optical, but steeper in the ultraviolet range (see Reimers et al. 1998) and compatible to the common assumption of $\alpha = -1.5$ for $\lambda \leq 1215$ Å.

4. The Lyman limit system at $z = 1.892$

As expected, the velocity profiles of Si II 1260, 1193, 1190, 1526, 1304, Si III 1206, Si IV 1393, 1402, C II 1334, C IV 1548, 1550 and Al II 1670 detected in the high-resolution optical spectra show a complex structure of the LLS at $z = 1.892$ (see Fig. 3). Inspection by eye of the velocity profiles reveals at least 11 different components spread over a velocity range of 200 km s^{-1}. The velocity offsets between the individual components range from 10 to 32 km s^{-1}. We have chosen the minimum number of components for which the fit of the complex cannot substantially be improved. The excellent coincidence between the total column densities derived from fitting of individual components with the total column densities obtained from the apparent optical depth method (Savage & Sembach, 1991) implies that there are no important contributions from hidden blended components unresolved at our resolution (but see Sect. 5 below). No edge leading asymmetry of the profiles is visible, as is found for the majority of damped Lyα absorbers (Wolfe 1995), favouring gaseous clumps instead of pointed motion like infall, outfall or rotation of gaseous clouds. Towards negative velocities absorption by low ions (C II and Si II) is dominating, while at the highest positive velocities absorption by highly ionized elements (C IV and Si IV) is dominating. Absorption lines of singly ionized elements show similar velocity profiles as do those of the high ions. The O I 1302 absorption line profile differs from those of the other elements, but it might be influenced by H I Lyα absorption.

No absorption is seen in the optical data for C I 1560, 1656, N I 1199, 1200, N V 1238, 1242, Si I 1631, 1845, Al I 1762, 1765, Mg I 1827, Zn I 1589 or Ni II 1741. Al III 1854 falls in a gap between the orders. Very weak and noisy absorption is visible for Al III 1862.

In the ultraviolet spectra prominent absorption by oxygen and carbon is visible, i.e. C II 903, C III 977 and O II 834, O III 507, 702, 832 and O IV 787 (see Fig. 4). O V 629 is located at the Lyman edge of the LLS at $z = 0.9756$. A strong absorption line with perfect wavelength agreement is also detected for O VI 1031, but, unfortunately, O VI 1037 is located in a complex blend. Weak absorption at the expected positions of N II 1084, N III 685, 685.5 and N IV 765 resonance lines is visible, too.

Further interesting ions which are only seen in absorption in the UV part of QSO spectra are those of neon and sulphur. Both lines of the Ne III 488, 489 doublet are located at the edge of a blend. Unfortunately, Ne IV 543, 542, 541, Ne V 568 and Ne VI 399, 401, 558 resonance lines fall in noisy regions of the spectrum. Ne V 480 might arise in a blend with O III 702 of the LLS at $z = 0.9756$. Absorption by Ne VII 465 is possible at the edge of a blend. Absorption lines detected at the expected positions of Ne VIII 770, 780 are offset by 0.43 and 0.65 Å, respectively, and are more likely identified with hydrogen lines. Regions of the spectrum were sulphur lines are expected are also shown in Fig. 4. S VI 933, 944 lines are located in blends.

5. Column density measurements

Fitting of absorption lines with Voigt profiles was done interactively using FIT/LYMAN in MIDAS to estimate column densities and line widths b. Different lines from the same ion were fitted simultaneously, but we fitted different elements and different ionization stages independently. We did not fit the 11 components simultaneously, instead we selected regions for individual fitting, i.e. the three components at the highest redshifts were always fitted simultaneously but independently of the other components.

The C IV 1548 absorption profile is blended with C IV 1550 absorption from the complex absorber system at $z = 1.8873$. A comparison of the Si II line profiles reveals that Si II 1190, 1193 must be blended, too. We did not try to fit the saturated region of Si III absorption. For component 4 we omitted fitting of Si IV and C IV because the data yield no useful constraints. For some components we fitted O I 1302 absorption, but since it shows a different velocity profile it might arise in a different gas phase or might be contaminated by H I Lyα absorption. The regions of corresponding Lyα, Fe II 1608 and N V 1238 absorption are just shown for comparison in Fig. 3.

A comparison of the fit results in Fig. 3 with the observations might hint at further hidden components. There seems to be an additional component at $+20$ km s^{-1} when inspecting C IV, C II and Si II absorption lines. The logarithmic column densities, Doppler parameters and redshifts for the individual components

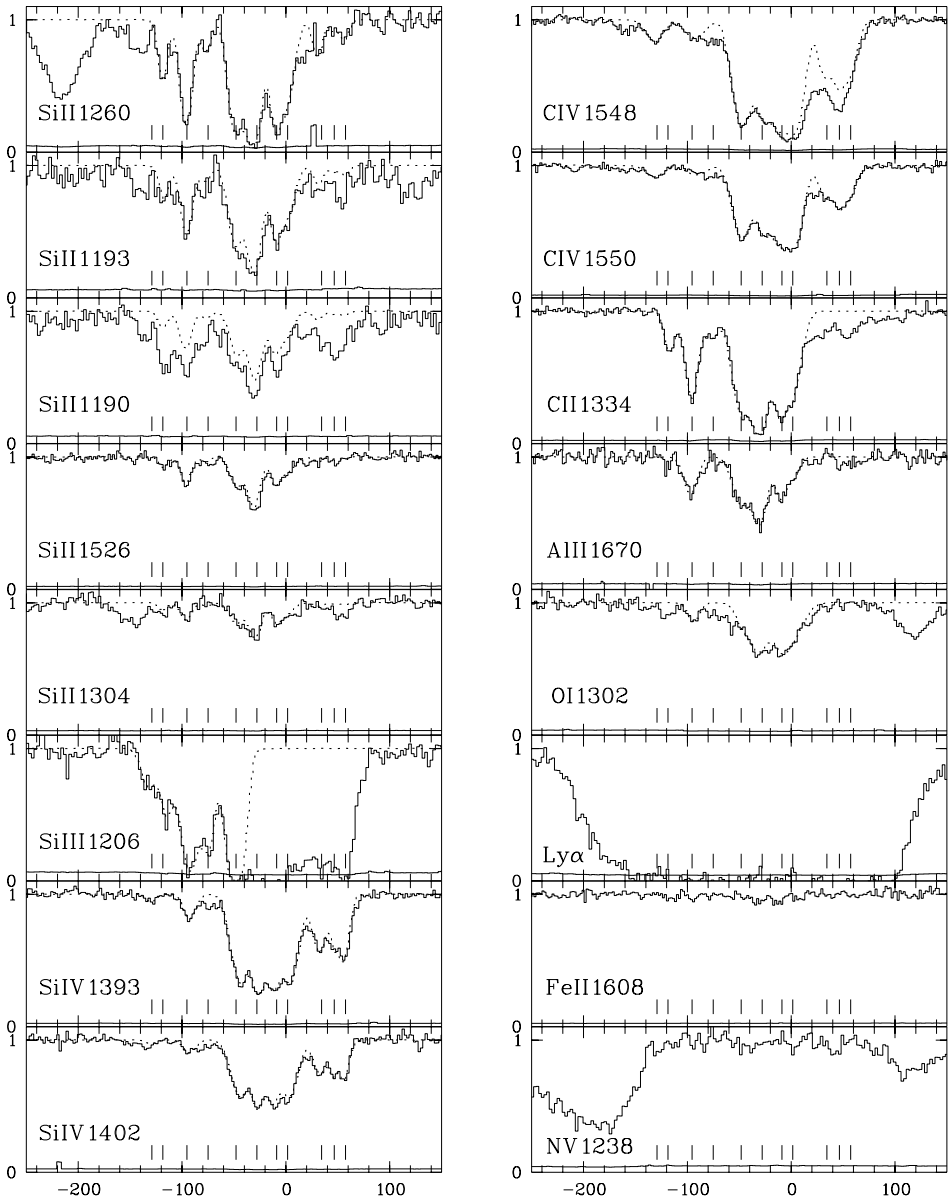

Fig. 3. Velocity profiles of Voigt profile fits (dotted lines) to absorption lines of the $z = 1.892$ LLS in optical spectra of HS 1103+6416. The $1\,\sigma$ error for the normalized flux is given, too. The ticks mark the positions of individual components. $v = 0\,\mathrm{km\,s^{-1}}$ corresponds to $z = 1.8920$. The C IV 1548 absorption profile is blended with C IV 1550 absorption from the complex absorber system at $z = 1.8873$. A comparison of the Si II line profiles reveals that Si II 1190, 1193 must be blended, too.

are listed in Table 2. Derived values are uncertain due to intrinsic line blending, the unknown number of components involved and the line fitting process by itself, since the fit results are not unique. The velocities v of the components are given relative to $z = 1.8920$. However, the total column densities derived for each ion in the high, intermediate, and low ionization groups respectively coincide remarkably well with the respective column densities measured by the apparent optical depth method (to within dex $\pm$ 0.15).

We fitted different ions independently with the intention to examine possible systematic changes in line widths or redshifts. Different b- and z-values of different ions of the same element could hint at an origin in gas phases with different ionization mechanisms, i.e. collisional ionization, photoionization by local sources or the extragalactic radiation field. Furthermore, the differences in b-values for different elements of the same component can yield the contributions of turbulent and/or thermal broadening of the lines.

For the following discussion of redshifts and b-values we will neglect the observed O I 1302 absorption. The errors in the central wavelengths as given by FIT/LYMAN are normally 0.01–0.02 Å, with a maximum error of 0.03 Å. We find differences in z up to 5 10^{-5} for lines of the same component. We do not find a systematic trend in redshift with ionization level, except for components 6, 7 and 8, where C IV and Si IV lines differ in redshift from the singly ionized elements. But especially these components are strongly blended and the ions might differ in the number of components involved.

Much more difficult is the derivation of the line widths. More than half of the b-values are marked by a colon which indicates that the fit error was greater than $1\,\mathrm{km\,s^{-1}}$. For the most reliable fits no systematic trend is found for b-values for ions of different ionization level which must mean that the line

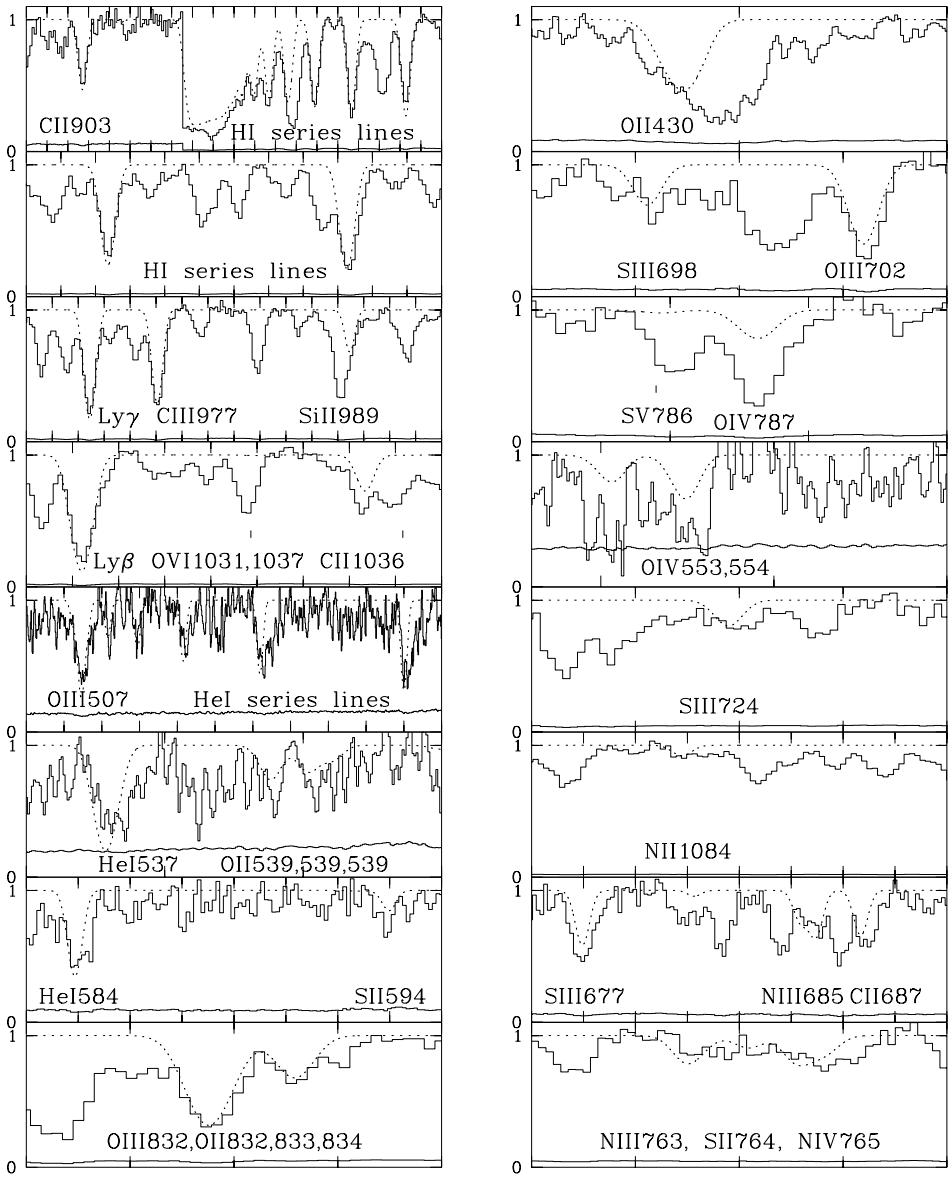

Fig. 4. The dotted lines represent the model results for the strongest absorption lines of the $z = 1.892$ LLS in the ultraviolet spectra of HS 1103+6416. The $1\,\sigma$ error for the normalized flux is given, too. The x-axis is given in Å with 5 Å distance between the tickmarks. The expected positions of O VI 1031, 1037 and S V 786 absorption lines are indicated by tickmarks.

widths are dominated by nonthermal components. The b-values are not particularly sensitive to the fitting procedure since, as can be seen from Fig. 3, it is always the combination of lines on different parts of the curve of growth that determines the b-values, even in case of SiIV and CIV where the line strengths of the doublet components are sufficiently different (not saturated). The main source of error is the insufficient S/N of the spectra, in particular for the weaker lines.

If there was a tail of shock-heated gas at high temperatures away from the curve of photoionization (Haehnelt et al. 1996), it should manifest itself in higher b values in CIV, which is not seen, or in NV (not seen) and OVI absorption. OVI absorption is probably seen (Fig. 4) although not unambiguously identified due to its location in the Ly α forest, which cannot be explained by photoionization and which indeed could be what Haehnelt et al. (1996) have predicted.

Especially for the weaker lines a much better signal-to-noise ratio would improve this analysis. However, if the complex line profiles are due to spatial correlations in stochastic velocity fields (so called mesoturbulence) the b-values derived by standard Voigt profile fitting could be grossly in error (see Levshakov et al. 1997 and references therein).

5.1. The ionization of the clouds

The maximum temperature derived from the largest b-value of Si IV in component 5 (C IV in component 1) is $2\ 10^5$ K ($8\ 10^4$ K) when assuming pure thermal broadening. At a temperature of $2\ 10^5$ K, C II should be completely destroyed by collisional ionization (Sutherland & Dopita 1993). But for component 5 strong C II absorption is visible, so that there is bulk motion in addition to thermal motion and the gas is rather photoionized. A hot, highly ionized phase does not seem to exist, otherwise

Table 2. Column densities of 11 components of the LLS in comparison to model results for different radiation fields. f indicates that the value was fixed. A colon indicates an error $> 1\,\mathrm{km\,s^{-1}}$. M1: power law, $\alpha = -1.5$; M2: Haardt & Madau (1996); M3: power law, $\alpha = -0.5$, factor 10 break.

C/v		O I	Si II	Si III	Si IV	C II	C IV	Al II	H I	log n_H	[C/H]	[Si/H]
1	z			1.89073	1.89075		1.89073					
−129	b			7.8:	5.1:		10.5					
	N			12.01	11.58		12.68					
M1	N	9.23	10.87	12.01	11.60	12.05	12.68	10.18	15.0	−2.9	−1.21	−1.1
M3	N	9.86	11.18	12.10	11.58	12.06	12.21	10.38	15.0	−2.37	−1.0	−0.72
2	z		1.89086	1.89089		1.89087						
−118.6	b		4.3	7.0:		5.4						
	N		12.28	12.31		13.03			16.05			
M1	N	12.02	12.28	12.31	10.90	13.03	10.90	11.02	16.05	−1.74	−1.07	−0.66
M3	N	11.92	12.21	12.32	11.11	12.99	11.29	11.14	16.05	−1.65	−1.0	−0.72
3	z	1.89109	1.89107	1.89110	1.89110	1.89108	1.89111	1.89107				
−95	b	6.4:	5.8	7.6:	6.5	6.4	13.0:	7.4:				
	N	13.1	12.76	12.92	12.19	13.55	12.66	11.80	16.53			
M1	N	12.09	12.72	13.28	12.35	13.58	12.60	11.80	16.53	−2.15	−1.17	−0.77
M3	N	12.15	12.74	13.15	12.21	13.56	12.51	11.79	16.53	−1.88	−1.0	−0.72
4	z		1.89126	1.89128		1.89127						
−75	b		5.2:	7.4:		8.1:						
	N		11.94	12.65		12.92			15.71			
M1	N	11.02	11.94	12.71	11.93	12.92	12.41	10.94	15.71	−2.35	−1.04	−0.72
M3	N	10.93	11.95	12.66	11.98	12.92	12.58	10.89	15.71	−2.16	−0.84	−0.68
5	z	1.89155f	1.89154	1.89154	1.89158	1.89155	1.89154	1.89153				
−48	b	8.5f	7.7	6.4:	10.9	10.6:	10.4	9.8:				
	N	13.1	12.92	13.64	13.09	13.83	13.63	12.01	16.70			
M1	N	11.75	12.92	13.80	13.16	13.83	13.61	12.02	16.71	−2.45	−1.12	−0.74
M3	N	11.83	12.91	13.68	13.05	13.83	13.60	12.00	16.71	−2.2	−0.95	−0.72
6	z	1.89171	1.89171		1.89174	1.89171	1.89174	1.89171				
−26	b	12.7:	6.8		5.2	7.5:	7.5:	8.4:				
	N	13.8	13.15		12.92	14.0	13.42	12.17	16.92			
M1	N	12.24	13.13	13.86	13.09	14.01	13.41	12.17	16.94	−2.3	−1.17	−0.77
M3	N	12.30	13.15	13.76	13.00	14.00	13.39	12.16	16.92	−2.05	−1.0	−0.72
7	z	1.89191	1.89190		1.89188	1.89189	1.89189	1.89190				
−8.9	b	7.9:	5.0:		7.1:	5.2:	8.9:	5.1:				
	N	13.38	12.71		12.99	13.53	13.57	11.74	16.48			
M1	N	11.36	12.71	13.68	13.11	13.52	13.54	11.74	16.49	−2.57	−1.23	−0.74
M3	N	11.44	12.68	13.56	13.00	13.53	13.54	11.74	16.49	−2.3	−1.03	−0.71
8	z	1.89201	1.89200		1.89204	1.89199	1.89204	1.89201				
1.6	b	14.1:	8.8:		9.1	10.4:	9.2	7.2:				
	N	13.66	12.69		13.02	13.72	13.63	11.52	16.46			
M1	N	11.44	12.71	13.62	13.01	13.73	13.61	11.52	16.47	−2.5	−0.99	−0.71
M3	N	11.49	12.69	13.51	12.94	13.72	13.64	11.53	16.47	−2.26	−0.81	−0.69
9	z		1.89230		1.89231		1.89231					
34	b		4.6:		7.4		6.5:					
	N		12.00		12.68		13.01					
M1	N	10.41	12.00	13.05	12.53	12.75	13.02	11.14	15.75	−2.7	−1.27	−0.72
M2	N	10.27	11.99	13.10	12.68	12.69	13.01	11.23	15.75	−2.75	−1.22	−0.72
M3	N	10.06	11.90	13.02	12.67	12.31	13.02	11.07	15.75	−2.65	−1.5	−0.72

Table 2. (continued)

C/v		O I	Si II	Si III	Si IV	C II	C IV	Al II	H I	log n_H	[C/H]	[Si/H]
10	z		1.89244		1.89244		1.89243					
46	b		0.7:		1.0:		5.5:					
	N		11.31		12.57:		12.93		15.08			
M2	N	8.94	11.29	12.50	12.27	12.01	12.91	10.37	15.08	−3.08	−1.22	−0.72
M3	N	8.61	11.31	12.49	12.32	11.66	12.93	10.05	15.08	−3.0	−1.44	−0.42
11	z		1.89254		1.89254		1.89253					
57	b		3.9:		5.0		9.0:					
	N		11.67		12.67		13.12		15.44			
M2	N	9.46	11.67	12.87	12.60	12.37	13.15	10.79	15.44	−3.0	−1.22	−0.72
M3	N	8.97	11.68	12.86	12.68	11.68	13.12	10.42	15.44	−3.0	−1.61	−0.42

we would expect to see absorption by N V or Ne VIII. We do see absorption at the expected positions of O VI 1031, 1037, but the identification is doubtful due to a possible contamination by H I Lyα. On the other hand, Kirkman & Tytler (1997) detected O VI and C IV but no N V absorption in a subcomponent of a LLS at $z = 3.3816$ and concluded that this component is rather collisionally ionized than photoionized.

From b(C IV)$= 5.5\,\mathrm{km\,s^{-1}}$ follows a maximum temperature of 22 000 K. Since at such low temperatures no C IV will be formed by collisional ionization (Sutherland & Dopita 1993) we will examine photoionization models for all components of the LLS.

Already from inspection by eye we notice different ionization levels in the components. Line profiles show strong absorption by singly and doubly ionized species but very weak absorption of highly ionized species for component 3. For components 9, 10 and 11 one can see that C II and Si II absorption is much weaker compared to other components, but C IV and Si IV are still strong. Component 6 shows in comparison to components 5, 7 and 8 stronger absorption by singly ionized species. In Table 3 we list the observed column density ratios like Si IV/C IV, Si III/Si IV etc. for the 11 individual components of the LLS at $z = 1.892$.

In the immediate neighbourhood of the LLS at $z = 1.892$ we find further complex MLSs at $z = 1.887$ and 1.942, i.e. with velocity differences of 500 and 5000 km s^{-1}, respectively. For comparison with the LLS at $z = 1.892$ we performed Voigt profile fits to all heavy element absorption lines detected longward of Lyα in emission. We identified in total 5 MLSs with redshifts between $z = 1.72$ and 2.05, 3 of which split into subcomponents. Results for the column densities and column density ratios are given in Table 4. We find that the ratio Si IV/C IV shows strong variations not only for the components of the LLS (see Table 3) but also for all these MLSs with absorption lines located longward of Lyα emission. Such variations are also detected for weaker MLSs at redshifts $z = 1.9$ up to 3.5 (see Boksenberg 1997). However, Boksenberg (1997) could not confirm the change in the column density ratio Si IV/C IV for Lyα clouds near $z = 3.1$ as found by Songaila & Cowie (1996). A generally low Si IV/C IV ratio of the order of 0.03 as claimed by Songaila & Cowie (1996) for Lyman forest clouds with $z < 3.1$ cannot be confirmed. This may be considered as evidence for additional ionizing mechanisms in MLS compared to Lyα clouds.

Table 3. Logarithmic column density ratios for the 11 individual components of the LLS at $z = 1.892$.

C	C II/C IV	Si III/Si IV	Si IV/C IV	O I/C II	Si II/Si IV	Si II/Si III
1		0.43	−1.1			
2						−0.03
3	0.89	0.73	−0.47	−0.45	0.57	−0.16
4						−0.71
5	0.2	0.55	−0.54	−0.73	−0.17	−0.72
6	0.58		−0.5	−0.2	0.23	
7	−0.04		−0.58	−0.15	−0.28	
8	0.09		−0.61	−0.06	−0.33	
9			−0.33		−0.68	
10			−0.36		−1.26	
11			−0.45		−1.0	

To estimate the ionization level of the individual components of the LLS at $z = 1.892$ we first simply compared our observed column density ratios like C II/C IV, Si III/Si IV, Si IV/C IV, O I/C II given in Table 3 with the diagrams shown by Bergeron & Stasinska (1986). From their photoionization calculations they noted that the ratio Si III/Si IV is almost independent of the H I column density and is therefore a good indicator of the ionization parameter U. Unfortunately, Si III is heavily saturated and blended for most of the components of the LLS. A reliable ratio Si III/Si IV is obtained only for components 1, 3 and 5. For the highly ionized components 9, 10 and 11 information is available only for the Si IV/C IV and Si II/Si IV ratios. Since the ratio Si IV/C IV also depends on the relative metal abundances we have chosen the ratio Si II/Si IV to constrain U or – when calculating photoionization models (see Sect. 6.1.1) – the hydrogen density.

For component 3 both C II/C IV and Si III/Si IV ratios hint at a cloud of low ionization with U between 2 10^{-3} and 2 10^{-4}. For component 5 both ratios indicate a cloud of slightly higher ionization than component 3 with U slightly below 2 10^{-3}. The O I/C II ratios do not fit into these models. Possible explanations are either differences in the relative abundances or different gas

Table 4. Column densities and column density ratios, both logarithmic, for 5 MLSs with heavy element absorption lines detected longward of Lyα emission. 3 of them reveal a splitting in subcomponents. For comparison column density ratios for the LLS at $z = 1.892$ are given in Table 3. f indicates that the value was fixed. A colon indicates an error $> 1\,\mathrm{km\,s^{-1}}$.

	H I	Si III	Si IV	C II	C IV	Si IV/C IV	Si III/Si IV	C II/C IV
z	1.71921		1.71935		1.71935			
b	48.4:		9.6		10.2			
N	16.87		12.67		13.00	−0.33		
z	1.84084				1.84084			
b	16.1				6.3			
N	13.49				13.65			
z		1.88720	1.88720f		1.88720			
b		4.0:	11.5:		12.1:			
N		11.82	12.08		13.48	−1.4	−0.26	
z		1.88733	1.88738f		1.88738			
b		4.3:	12.4:		12.5			
N		11.86	11.71		13.26	−1.55	0.15	
z		1.88761	1.88762		1.88762f			
b		5.5	5.9:		8.4			
N		11.51	11.79		13.36	−1.57	−0.28	
z		1.94065	1.94063		1.94064			
b		5.4:	4.7:		2.5			
N		11.56	12.04		12.72	−0.68	−0.48	
z		1.94099	1.94097		1.94101			
b		14.4:	17.5:		28.9			
N		12.47	12.55		14.01	−1.49	−0.08	
z		1.94106	1.94105	1.94105	1.94105			
b		3.9:	4.3	7.5:	6.5			
N		12.64	12.94	12.65	13.95	−1.01	−0.3	−1.3
z		1.94135	1.94133		1.94132			
b		4.3:	6.0:		6.1			
N		11.75	12.03		13.28	−1.25	−0.28	
z					2.04563*			
b					7.0			
N					13.34			

* At least two components according to Lyα.

phases. For components 9, 10 and 11 Si IV/C IV ratios are a little bit higher than in the neighboring components of the same LLS. Si IV/C IV ratios are also much stronger compared to the neighbouring complex absorption line systems at $z = 1.88$ and 1.94 (see Table 4). Either these systems are not exposed to the same ionizing radiation field or they differ in element abundances. Also, the Si II/Si IV ratio of component 9 is much lower than in other LLS components. Values for Si II and Si IV column densities in components 10 and 11 are much more uncertain, but indicate also high ionization.

Components 5, 7 and 8 are of intermediate ionization according to their column density ratios. Less information is available for components 1, 2 and 4. According to the Si II/Si III ratio component 4 is comparable to component 5 and component 2 is rather comparable to component 3. The Si III/Si IV ratio of component 1 yields a low ionization with U slightly below $2\,10^{-3}$.

To perform model calculations we need to know the H I column densities of the individual components. Since O I can arise in a different gas phase, i.e. a mainly neutral phase, and the observed O I profile does not follow the profiles of the singly ionized elements we chose Si II as a tracer of the H I column density. From the Lyman edge in HST data we find a total H I column density of $\log N(\mathrm{H\,I}) = 17.46\,\mathrm{cm^{-2}}$. From the apparent optical depth method (see Savage & Sembach 1991) we find a total Si II column density $\log N(\mathrm{Si\,II}) = 13.69\,\mathrm{cm^{-2}}$. H I column densities for the individual components are derived according to the ratios of the observed Si II column densities in the individual components to the total Si II column density. The total column density of the 11 components is then $\log N(\mathrm{H\,I}) = 17.40\,\mathrm{cm^{-2}}$. The remaining hydrogen column density of 3.6 $10^{16}\,\mathrm{cm^{-2}}$ might be related to the O I absorption. Results for $\log N(\mathrm{H\,I})$ are given in Table 2.

6. Photoionization models

In order to estimate the ionization state of the absorbing clouds, photoionization models have been calculated using Ferland's program CLOUDY (Ferland 1993). The absorber clouds were

modelled as plane-parallel slabs of constant density, illuminated on one side by the ionizing radiation field. Solar abundances specified by number relative to hydrogen as given by Gehren (1988) were used: He: 0.1, O: 8.32 10^{-4}, C: 4.68 10^{-4}, N: 9.77 10^{-5}, Mg: 3.98 10^{-5}, Si: 3.72 10^{-5}, Fe: 3.39 10^{-5}, S: 1.86 10^{-5}, Ar: 6.31 10^{-6}, Al: 3.16 10^{-6}, Ca: 2.29 10^{-6}, Na: 2 10^{-6}, Ni: 1.78 10^{-6}. The solar neon abundance 1.26 10^{-4} from Grevesse & Anders (1989) was chosen instead of the uncertain Ne abundance 6.3 10^{-5} given by Gehren (1988).

For the intensity of the ionizing background at the Lyman limit Haardt & Madau (1996) found from model calculations 4 10^{-22} erg s^{-1} cm^{-2} Hz^{-1} sr^{-1} at $z = 1.8$, while Bechtold found 3 10^{-21} erg s^{-1} cm^{-2} Hz^{-1} sr^{-1} (Bechtold 1994) for $1.6 < z < 4.1$ using the proximity effect. We adopt throughout $\log J_\nu = -22$ erg s^{-1} cm^{-2} Hz^{-1} sr^{-1}. If the flux at the Lyman limit is indeed a factor 30 larger as demanded by the proximity effect we have to choose a 30 times higher density resulting in smaller cloud sizes.

The H I column density was fixed to the value derived from Si II (see Sect. 5) and the total hydrogen density was varied until the best agreement with the column density ratios was found.

We tried several radiation fields: a) a simple power law with $\alpha = -1.5$ (model M1), b) the radiation field calculated by Haardt & Madau (1996) at $z = 1.8$ (model M2) or c) a power law with $\alpha = -0.5$ and a break by a factor of 10 at the He II ionization edge to account for absorption by intervening absorber systems (model M3; see Fig. 5). C, Si and Al abundances were chosen individually dependent on the radiation field.

6.1. Description of model results

6.1.1. Results on carbon, silicon and aluminum

In Table 2 model results for the different radiation fields are compared with the observed column densities. Errors in the derived column densities as given by FIT/LYMAN are normally in the range from 0.02–0.12 dex, but larger variations might exist between different fit results for a single line. For the "low ionization" components 3 and 6 best agreement is found for model M3. The Haardt & Madau (1996) model (M2) is too soft and does not produce enough C IV. The simple power law with $\alpha = -1.5$ overestimates Si III and Si IV. C and Si abundances are identical for both components ([C/H] $= -1$, [Si/H] $= -0.72$), but the Al abundances differ slightly. Since component 2 appears also of low ionization it was fitted with M3 and is well reproduced with the abundances found for component 3. For component 1 the H I column density is unknown, but H I and the hydrogen density have been varied for the radiation field M3 and abundances as given above until the Si II/Si III ratio was reproduced, but then C IV is underestimated. Unless we know the C II column density we are not able to decide between differences in the carbon abundance and the ionizing mechanism.

For the highly ionized components we used the ratio Si II/ Si IV to constrain the hydrogen density. The carbon abundance was then varied until the observed C IV column density was reproduced. For component 9 best agreement is found for model M2. The carbon abundance is slightly smaller than found for the components of low ionization, but the Si abundance is identical. Also, the better representation of C II favours the radiation field as calculated by Haardt & Madau (1996). For component 10 the same parameters yield satisfactory agreement for Si II and C IV, but a too small Si IV column density. However, the observed value of Si IV is quite uncertain. Nearly similar results are obtained for the radiation field M3 when adopting lower C and Si abundances. The relative abundances [Si/C] obtained for the latter model are then larger by a factor of ≈ 2. For component 11 we find similar results as for component 10. As can be seen in the calculation for component 9 the simple power law with $\alpha = -1.5$ (model M1) has problems in reproducing the Si IV column density.

Components 4, 5, 7 and 8 of intermediate ionization are also best reproduced adopting model M3 but with different abundances [C/H] and [Si/H]. For components 4 and 5 model M1 is overestimating Si III.

Components of low and intermediate ionization (components 2 to 8) show a smaller Si overabundance relative to C ([Si/C] $= 0.12$, 0.16, 0.23, 0.28, 0.32) in comparison to 0.5 for the highly ionized components. If all components were ionized by the same radiation field (model M3) the [Si/C] overabundance would be even larger for the highly ionized components. The aluminum abundance is nearly the same for all models. It was varied between [Al/H] $= -0.97$ and -1.17 in order to reproduce the observed Al II column density with the exception of component 8, where [Al/H] $= -1.3/-1.34$ had to be chosen. No overabundance of Al with respect to C is found, but no measurements of Al II are available for the highly ionized components. However, a $3\,\sigma$ upper limit for the Al II equivalent width of component 9 yields [Al/H] ≤ -1.25 and thus [Al/C] ≤ -0.03. The derived Al abundances agree well with the results found for Halo stars: no overabundance of Al relative to Fe is found at [Fe/H] $= -1$ and the ratio [Al/Fe] is decreasing with decreasing [Fe/H] while Si is overabundant relative to Fe with a mean ratio [Si/Fe] of 0.5 (McWilliam et al. 1995).

6.1.2. Results on oxygen, nitrogen and sulphur

Abundances of N, O, S and Ne are in principal constrained by absorption lines observed in the ultraviolet. Due to the low resolution we could not derive individual abundances, but adopted instead common values for all components. As mentioned above all neon lines are located in strong blends, thus, the neon abundance was set to [Ne/H] $= -0.7$ as found for [Si/H] in most components. The oxygen abundance is determined by several O II and O III lines. Only weak absorption is visible for N and S, thus, the resulting abundances are stronger influenced by the chosen continuum level. All other abundances were set to one tenth their solar values.

For comparison of the model results with the HST spectra we need information about the line broadening mechanism. No uniform b-values were found for the different elements. Most reliable b-values or the mean of the measured b-values of carbon and silicon were taken to derive turbulent und thermal velocity

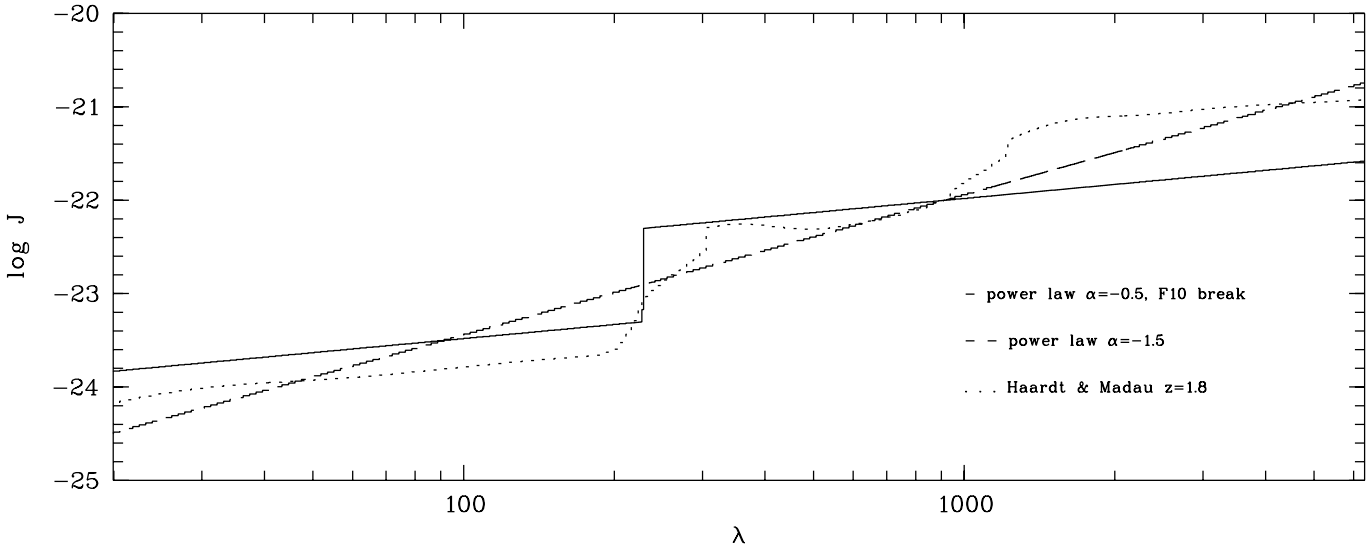

Fig. 5. Radiation fields adopted in the photoionization models. The solid line represents a power law with $\alpha = -0.5$ and a break by a factor of 10 at the He II ionization edge (model M3). The dashed line is a simple power law with $\alpha = -1.5$ (model M1). The dotted line yields the radiation field calculated by Haardt & Madau (1996) at $z = 1.8$ (model M2). J is given in erg s^{-1} cm^{-2} Hz^{-1} sr^{-1}.

parameters. For components 10 and 11 we take the values found for component 9, because the measured values yield no meaningful results. For half of the components (4, 5, 6, 7 and 9) the derived temperatures are then in the range 25 000–33 000 K. These temperatures are consistent with those found in the CLOUDY photoionization calculations. For component 1 we find a very high temperature of 65 000 K, but the silicon b-values are poorly determined. For component 3 and 8 we find very low temperatures of 2000 and 3800 K, respectively, but the b-values are also poorly constrained. For all components we have to introduce an additional turbulent component with values between 2–12 km s^{-1}.

With the parameters derived from the optical data we started the model calculations for all 11 components with very small O, N and S abundances. A UV spectrum is then synthesized from the model results with individual b-values as mentioned above and convolved with the instrumental profile for comparison with the UV observations (see Fig. 4). The observed C III 977 and C II 903.6, 903.9 absorption is well explained by the model parameters derived from the optical absorption lines. The O III 832, O II 833, 834, 832 and O III 702 resonance lines are well reproduced for [O/H] $= -0.85$. As can be seen from the 1 σ noise level in Fig. 4 O IV 553, 554, O III 507, O II 539.0, 539.5, 539.8 and He I series lines are located in noisy regions with uncertain continuum definitions. This might be the reason why the predicted absorption is slightly stronger than observed. S III 677 is blended with Lyα at $z = 0.6122$ and Si II 989 is blended with Lyγ of the MLS at $z = 1.94$. S III 724 and S II 765, 764, 763 yield [S/H] $= -0.8$. In the presence of dust we expect null depletion for S as it is found in the Galaxy, while Si should be strongly affected. The ratio [S/Si] $= -0.08$ derived for the low ionization components hints at the absence of noticable amounts of dust.

With [N/H] $= -1.5$ the predicted absorption is too weak in comparison with the observations, while [N/H] $= -1$ predicts slightly too much absorption in case of N III 685, 685.5, 763 (see Fig. 4). But due to the high line density and the low resolution the continuum level might be underestimated.

With the O abundance determined from the UV absorption lines of O II and O III, our models cannot reproduce the observed O I absorption. In order to explain the O I absorption one has to invoke further mainly neutral components with relatively low H I column densities. Also, the photoionization models do not predict significant absorption by O VI. However, if the observed absorption is indeed O VI there is still the possibility of a collisionally ionized phase as found in our Galaxy. Kirkman & Tytler (1997) favoured collisional ionization for a component with strong O VI and C IV absorption in a LLS at $z = 3.3816$, too. Since for the "highly ionized" components (9, 10 and 11) in the LLS at $z = 1.892$ we do detect absorption by C II, the observed C IV absorption might be related to both a collisionally ionized and a photoionized phase, thereby making model calculations more difficult.

6.1.3. Results on helium

Absorption lines of neutral helium were first discovered in HST spectra of the UV-bright, high-redshift ($z = 2.72$) QSO HS 1700+6416 (Reimers & Vogel 1993). Ultraviolet spectra of the $z = 2.13$ QSO HS 1307+4617 also reveal He I 584, 537, 522 absorption lines for all LLS with a suitable redshift. We found column density ratios N(H I)/N(He I) of 35 to 43 adopting turbulent line broadening and 4 to 10 for pure thermal line broadening, respectively (see Reimers et al. 1998).

Both the absence of knowledge of the splitting into subcomponents and the unknown ionization conditions, however, made

it impossible to perform a more quantitative analysis of He I lines, e.g. in terms of the He abundance.

For the LLS discussed here He I resonance series lines up to He I 508 are clearly visible in the UV spectra. In our model calculations for the 11 components we fixed the He abundance He/H to 0.079 ($Y = 0.24$) and found surprisingly good agreement between the synthesized and the observed spectrum (see Fig. 4), although the predicted absorption is throughout a little bit stronger than the observed one. According to the photoionization models column density ratios $N(\mathrm{H\,I})/N(\mathrm{He\,I})$ for the components of low and intermediate ionization range from 13.5 to 15 and 16.6 to 18.2, respectively. For the highly ionized components we found ratios of 21, 31 and 35.

It can also be seen from Fig. 4 that in comparison with the synthesized spectrum the observed He I absorption lines all reveal an additional absorption component in the red wing ranging at least up to $v \approx 100\,\mathrm{km\,s^{-1}}$ relative to $v = 0\,\mathrm{km\,s^{-1}}$ ($z = 1.8920$). Also, from Fig. 3 it is obvious that Lyα and C II 1334 absorption is more extended to the red than indicated by the components identified. At $v = 120\,\mathrm{km\,s^{-1}}$ we detect absorption which might be related to O I 1302. A Voigt profile fit yields $N(\mathrm{H\,I}) = 12.91\,\mathrm{cm^{-2}}$ and $b = 21.7\,\mathrm{km\,s^{-1}}$ rather indicating a H I Lyα absorption line. A higher signal-to-noise ratio could help to distinguish between multiple O I 1302 absorption lines and Lyα forest absorption.

More quantitative constraints for the He abundance are difficult due to the low signal-to-noise ratio of the spectra. In combination with the blending problem at low resolution it is extremely difficult to reliably determine the continuum level. Having this in mind, the near agreement of model calculations with $Y = 0.24$ with the observed He I series can be considered as fully consistent with the expectation of big bang nucleosynthesis (see Boesgaard & Steigman, 1985). With the planned COS spectrograph on HST there is a chance to really measure the He abundance at $z = 2$.

7. Summary and discussion

We have studied a complex Lyman limit system at z = 1.9 towards the UV bright QSO HS 1103+6416 using a combination of ultraviolet HST spectra of low resolution with optical high-resolution spectra. This combination for the first time allows a quantitative study of abundances of several heavy elements (C, O, N, S, Si, S, Al) and of the ionization conditions by using the observed subcomponent splittings from the optical (CII, SiII, AlII,..) to synthesize lines from ions like OII, OIII, OIV, NII, NIII, SIII, etc.) at intrinsic EUV wavelengths.

We find that the complex absorption system that spans a velocity range of roughly $200\,\mathrm{km\,s^{-1}}$ with at least 11 components can be subdivided into three groups: A low ionization subgroup L: components 2, 3, 6 with radial velocities v = -129 to $-95\,\mathrm{km\,s^{-1}}$, an intermediate ionization group I: components 4, 5, 7, 8 (v = -75... $+2$), and a high-ionization subgroup H with components 9, 10, 11 (v = $+3.4$... $+57$). Component 1 at $-129\,\mathrm{km\,s^{-1}}$ appears to belong to group H.

Ionization calculations show, that ion ratios in components L (ionization parameter log U < -3.1) and I (log U = -2.9 to 3) are best fitted with a rather hard radiation field (M3; power law with $\alpha = -0.5$ and a break by factor 10 at the HeII edge) while for the high ionization component H the best fit is obtained with the metagalactic UV radiation background as predicted by Haardt & Madau (1996). The probable implication is that while the 'Halo' component H is purely photoionized by the metagalactic UV background, the low and intermediate ionization clouds, which possibly differ only in electron density, need an additional source of ionization, which cannot be local stars, since a harder radiation field compared to the Haardt & Madau (1996) UV background is required. This result and the detection of OVI, which cannot be produced by photoionization models, both provide evidence for collisional ionization as a further ionization mechanism or deviations from strict photoionization equilibrium (Rauch et al., 1997). Our results on ionization are similar to what Boksenberg (1997) has found in his study of strong metal line systems of the QSO HS 1626+6433 (Reimers et al. 1995a). Besides the systematic variation of ionization with velocity, we do see distinctive abundance differences, in particular between the high ionization components H on one hand and the low and intermediate ionization components L and I on the other hand.

For the 'Halo' components H we find [C/H] = -1.2 and for the α-elements O, Si and S roughly [α/C] = 0.4 $\pm$0.1, while [N/C] = 0.2. For oxygen, a similar overabundance at low metal abundances is known from both QSO absorption systems at z = 2 (Vogel & Reimers 1995) and from metal deficient stars (e.g. Israelian et al. 1998). This is in accordance with SNII nucleosynthesis in massive stars before lower mass stars contribute significantly to heavy element production (see McWilliam 1997).

Components L and I show [C/H] ≈ -1 and only slight ([Si/C] = 0.2) or no ([O/C] $\approx$ [S/C] $\approx$ [Al/C] $\approx$ 0) overabundance, within the uncertainties. This is still consistent with what is seen in the galactic disk at 1/10 solar abundance (Fig. 3a in McWilliam 1997).

If all components (L, I and H) were ionized by the same radiation field, the overabundance of Si relative to C would be even larger up to [α/C] = $+1$ in the highly ionized components, which is not consistent with what is known from metal deficient 'Halo' stars.

While the systematic trends of ionization and abundances with velocity, i.e. different locations in a galaxy or group of galaxies, appear to be real and consistent with evidence from other sources of information (Halo stars, QSO absorption line systems) we have to remember that neither the fit results nor the model results are quantitatively unambiguous.

Possibly both low and high ions are a mixture from different gas phases with different ionization mechanisms as found for the Milky Way (Savage 1987). In this case, the observed column density ratios cannot be used to constrain photoionization models. Also, the assumption of individual, isolated clouds producing absorption lines might be inadequate (see Miralda-Escudé et al. 1997).

Optical data of higher signal-to-noise are needed to obtain more reliable information on column densities and b-values especially for weak absorption lines, and higher resolution in the UV range provided in the future by the COS spectrograph will allow to improve constraints on the models via the large number of intrinsic EUV quasar absorption lines.

Acknowledgements. We are indebted to G. Ferland who provided us with his photoionization code CLOUDY. We thank the referee Chris Impey for his constructive remarks. This work has been supported by the Verbundforschung of the Bundesministerium für Bildung und Forschung under No. 50 OR 96 016.

References

Bechtold J., 1994, ApJS 91, 1
Bergeron J., Stasinska G., 1986, A&A 169, 1
Boesgaard A.M., Steigman G., 1985, ARA&A 23, 319
Boksenberg A., 1997, In: Petitjean P., Charlot S. (eds.) Structure and Evolution of the IGM from QSO Absorption Line Systems. Proc. 13th IAP Colloquium, Editions Frontières, Paris, 85
Ferland G.J., 1993, University of Kentucky Department of Physics and Astronomy Internal Report
Gehren T., 1988, Reviews in Mod. Astr. 1, 52
Grevesse N., Anders E., 1989, In: Waddington C.J. (ed.) Cosmic abundances of matter. AIP conference proceedings 183
Haardt F., Madau P., 1996, ApJ 461, 20
Haehnelt M.G., Steinmetz M., Rauch M., 1996, ApJ 465, L95
Hagen H.-J., Groote D., Engels D., Reimers D., 1995, A&AS 111, 195
Israelian G., Garcia Lopez R., Rebolo R., 1998, Astro-ph/980235
Kirkman D., Tytler D., 1997, ApJ 489, L123
Köhler S., Reimers D., Wamsteker W., 1996, A&A 312, 33
Levshakov S.A., Kegel W.H., Takahara F., 1997, In: Petitjean P., Charlot S. (eds.) Structure and Evolution of the IGM from QSO Absorption Line Systems. Proc. 13th IAP Colloquium, Editions Frontières, Paris, 414
Madau P., 1995, ApJ 441, 18
McWilliam A. 1997, ARA&A 35, 503
McWilliam A., Preston G.W., Sneden C., Searle L., 1995, AJ 109, 2757
Miralda-Escudé J., Rauch M., Sargent W.L.W. et al., 1997, In: Petitjean P., Charlot S. (eds.) Structure and Evolution of the IGM from QSO Absorption Line Systems. Proc. 13th IAP Colloquium, 155
Rauch M., Haehnelt M.G., Steinmetz M., 1997, ApJ 481, 601
Reimers D., Vogel S., 1993, A&A 276, L13
Reimers D., Vogel S., Hagen H.-J., et al., 1992, Nat 360, 561
Reimers D., Rodriguez-Pascual P., Hagen H.-J., Wisotzki L., 1995a, A&A 293, L21
Reimers D., Bade N., Schartel N., et al., 1995b, A&A 296, L49
Reimers D., Köhler S., Hagen H.-J., Wisotzki L., 1998, In: Harris R.A. (ed.) Ultraviolet astrophysics – Beyond the IUE final archive. Conf. proc. SP-413, ESA Publications Division, 579
Savage B.D., 1987, In: Blades J.C., Turnshek D.A., Norman C.A. (eds.) QSO absorption lines: Probing the Universe. Proc. of QSO absorption line meeting, Cambridge University Press, 195
Savage B.D., Sembach K.R., 1991, ApJ 379, 245
Seaton M.J., 1979, MNRAS 187, 73
Songaila A., Cowie L.L., 1996, AJ 112, 335
Sperhake U., Reimers D., 1997, In: Petitjean P., Charlot S. (eds.) Structure and Evolution of the IGM from QSO Absorption Line Systems. Proc. 13th IAP Colloquium, 448
Stark A.A., Gammie C.F., Wilson R.W., et al., 1992, ApJS 79, 77
Sutherland R.S., Dopita M.A., 1993, ApJS 88, 253
Vogel S., Reimers D., 1995, A&A 294, 377
Vogt S.S., Allen S.L., Bigelow B.C., et al., 1994, Proc. SPIE, 2198, 362
Weedman D.W., 1986, Quasar astronomy. Camb. Univ. Press
Wolfe A.M., 1995, In: Meylan G. (ed.) QSO absorption lines. Proc. of ESO Workshop, Springer, Berlin, p. 13